Free Radical Research

ISSN: 1071-5762 (Print) 1029-2470 (Online) Journal homepage: http://www.tandfonline.com/loi/ifra20

Radical-induced purine lesion formation is dependent on DNA helical topology

Michael A. Terzidis, Andreea Prisecaru, Zara Molphy, Niall Barron, Antonio Randazzo, Elise Dumont, Marios G. Krokidis, Andrew Kellett & Chryssostomos Chatgilialoglu

To cite this article: Michael A. Terzidis, Andreea Prisecaru, Zara Molphy, Niall Barron, Antonio Randazzo, Elise Dumont, Marios G. Krokidis, Andrew Kellett & Chryssostomos Chatgilialoglu (2016): Radical-induced purine lesion formation is dependent on DNA helical topology, Free Radical Research, DOI: 10.1080/10715762.2016.1244820

To link to this article: http://dx.doi.org/10.1080/10715762.2016.1244820

Accepted author version posted online: 13 Oct 2016.

Radical-induced purine lesion formation is dependent on DNA helical topology

Michael A. Terzidis,[a] Andreea Prisecaru,[b] Zara Molphy,[b] Niall Barron,[b] Antonio Randazzo,[c] Elise Dumont,[d] Marios G. Krokidis,[e] Andrew Kellett,[b]* and Chryssostomos Chatgilialoglu[a,e]*

[a] *ISOF, Consiglio Nazionale delle Ricerche, Via P. Gobetti 101, 40129 Bologna (Italy), Email: chrys@isof.cnr.it, Tel.: +39-051-6398309*

[b] *School of Chemical Sciences and National Institute for Cellular Biotechnology, Dublin City University, Glasnevin, Dublin 9 (Ireland), Email: andrew.kellett@dcu.ie, Tel.: +353-1-7005461*

[c] *Department of Pharmacy, University of Naples "Federico II", via D. Montesano 49, I-80131, Napoli (Italy)*

[d] *Laboratoire de Chimie, UMR 5182 CNRS, École Normale Supérieure de Lyon, 46, allée d'Italie, 69364 Lyon Cedex 07 (France)*

[e] *Institute of Nanoscience and Nanotechnology, NCSR "Demokritos", 15341 Agia Paraskevi, Athens (Greece),*

Radical-induced purine lesion formation is dependent on DNA helical topology

Abstract

Herein we report the quantification of purine lesions arising from gamma-radiation sourced hydroxyl radicals ($HO^{\bullet}$) on tertiary dsDNA helical forms of supercoiled (SC), open circular (OC) and linear (L) conformation, along with single-stranded folded and non-folded sequences of guanine rich DNA in selected G-quadruplex structures. We identify that DNA helical topology and folding plays major, and unexpected, roles in the formation of 8-oxo-7,8-dihydro-2'-deoxyguanosine (8-oxo-dG) and 8-oxo-7,8-dihydro-2'-deoxyadenosine (8-oxo-dA), along with tandem-type purine lesions 5′,8-cyclo-2′-deoxyguanosine (5′,8-cdG) and 5′,8-cyclo-2′-deoxyadenosine (5′,8-cdA). SC, OC, and L dsDNA conformers together with folded and non-folded G-quadruplexes $d[TGGGGT]_4$ (TG4T), $d[AGGG(TTAGGG)_3]$ (Tel22) and the mutated tel24 $d[TTGGG(TTAGGG)_3A]$ (mutTel24) were exposed to $HO^{\bullet}$ radicals and purine lesions were then quantified via stable isotope dilution LC-MS/MS analysis. Purine oxidation in dsDNA follows L > OC >> SC indicating greater damage toward the extended B-DNA topology. Conversely, G-quadruplex sequences were significantly more resistant toward purine oxidation in their unfolded states as compared with G-tetrad folded topologies; this effect is confirmed upon comparative analysis of Tel22 (~50% solution folded) and mutTel24 (~90% solution folded). In an effort to identify the accessibly of hydroxyl radicals to quadruplex purine nucleobases, G-quadruplex solvent cavities were then modelled at 1.33 Å with evidence suggesting that folded G-tetrads may act as potential oxidant traps to protect against chromosomal DNA damage.

Keywords: cyclonucleoside, DNA oxidation, hydroxyl radical, G-quadruplex, superhelix

Introduction

The hydroxyl radical ($HO^{\bullet}$) is a potent oxidant that reacts at near diffusion-limited rates with most biomolecules, including nucleic acids.[1] This radical is produced in biological systems through oxygen metabolism, however, several well recognised exogenous factors, *e.g.* exposure to ionising radiation or redox metal ion overload, are known to produce $HO^{\bullet}$ and related reactive oxygen species (ROS).[1] With regard to DNA chemical reactivity, diffusible $HO^{\bullet}$ are known to either add to base moieties,[2] with the majority of $HO^{\bullet}$ attacks occurring at this location, or abstract a H-atom from 2-deoxyribose units.[3] Indeed, given the proximity of deoxyribose C5′ toward the edge of the minor groove, H5′ abstraction by diffusible $HO^{\bullet}$ predominates over all other possible sugar positions with reactions at purine nucleosides (**1**), leading to tandem-type lesions of 5′,8-cdG and 5′,8-cdA (Scheme 1).[3,4] Both 5′,8-cdG and 5′,8-cdA lesions, in their 5′*S* (**2**) and 5′*R* (**3**) diastereomeric forms, are repaired at low efficiency by the human nucleotide excision repair (NER) pathway[5] with recent work demonstrating *ca*. 2 times greater efficacy for 5′*R* over 5′*S* diastereomer repair, owing to greater DNA backbone distortions encountered in 5′*R* diastereomeric lesion-containing sequences.[6] In contrast to sugar H-atom abstraction, $HO^{\bullet}$ attack on purine base moieties is widely known to generate lesions of 8-oxo-dG and 8-oxo-dA (Scheme 1, (**4**)) that impact on genome structural integrity, mutagenicity, excision repair, and polymerase fidelity.[2,7]

DNA lesion quantification methods, developed and extensively used within the last decade, are mainly based on liquid chromatography coupled with highly sensitive mass detectors. Although LC-MS/MS has been used to identify the yields of radiation-induced purine lesions of calf thymus DNA in aqueous solutions,[8] the quantification of purine lesions from gamma (γ)-irradiation sourced hydroxyl radicals on tertiary

superhelical double stranded (dsDNA) conformations—supercoiled (SC), open circular (OC), and linear (L)—have yet to be elucidated.

Scheme 1 here

The presence of molecular oxygen in the reaction of $HO^{\bullet}$ radicals with DNA can substantially change the reaction products and/or the mechanistic pathways. For example: (*i*.) under aerobic conditions (20% O_2 corresponds to 2.68 x 10^{-4} M, which is *ca*. 7 times higher than of typical well-oxygenated tissues, i.e., [O_2] ~0.04 mM),[9] about 50% of 8-oxo-dG and 8-oxo-dA are involved in tandem damage and are produced by base-derived peroxyl radicals that add onto C8 of a vicinal purine base,[10] and (*ii*.) the levels of 5′,8-cdG and 5′,8-cdA lesions were found to decrease steadily with an increase in O_2 concentration. [11] Competitive kinetic studies indicated the rate constant of C5′ radical cyclization (k_c) to the purine base to be ca. 2 x 10^4 s^{-1} in dsDNA (Scheme 2).[12]

Scheme 2 here

A detailed protocol revision for the quantification of the six purine lesions of DNA reported in Scheme 1 has been recently provided by some of us.[13] The quantification of radiation-induced purine lesions in single and double stranded calf thymus DNA and in the absence or presence of oxygen was performed too.[12] In particular, under physiological levels of oxygen (e.g., 6.7 x 10^{-5} M) the formation rates of 5′,8-cdG and 5′,8-cdA in dsDNA are similar and close to 0.08 lesions per 10^6 nucleotides per gray (Gy) with the formation of 8-oxo-dG and 8-oxo-dA being 280 and 30 times higher, respectively. Given the significance of oxidative DNA damage toward genomic strand breaks and mutagenic nucleobase modification, the current work

presents a model which shows for the first time how DNA helical topology and G-quadruplex folding influences $HO^{\bullet}$ induced purine lesion formation. To that end, we report how 8-oxo-dG, 8-oxo-dA, and tandem-type 5′,8-cdG, and 5′,8-cdA lesions, generated via γ-radiation sourced $HO^{\bullet}$ under physiological levels of oxygen, are directly influenced by tertiary dsDNA helical form. To identify lesion formation within dsDNA helical forms, supercoiled plasmid DNA—a substrate that mimics, in many ways, the conformation of histone-wound supercoiled genomic DNA found within mammalian cells [14,15] was employed. The structural and energetic status of 5′,8-cdG and 5′,8-cdA lesions has recently been studied in nucleosomes along with DNA-histone interactions and local electrostatic potentials, with emphasis on the hydrogen bond between Lys115 of histone H3 and the DNA backbone which has been observed in the case of cdG lesions. [16] Secondly, given the importance of non-coding repeat guanine-rich sequences found in the telomeric ends of chromosomes,[17,18] allied with recent discovery of G-quadruplex formation with human telomeres, [19] purine lesion frequency within folded and unfolded G-quadruplex states were identified. Three DNA G-rich sequences capable of forming G-quadruplex structures in solution, namely $d[TGGGGT]_4$ (TG4T),[20] $d[AGGG(TTAGGG)_3]$ (Tel22),[21,22] and the mutated tel24 $d[TTGGG(TTAGGG)_3A]$ (mutTel24)[23] were synthesised and characterized by NMR prior to γ-irradiation. NMR studies on these quadruplex structures reveal that TG4T is folded into a tetramolecular parallel quadruplex.[20] On the contrary, Tel22 is folded into monomeric antiparallel quadruplex,[21] while mutTel24 into a so-called hybrid structure,[23] where three strands are parallel to each other and one antiparallel. This provided us a platform to probe purine lesion formation in the context of both nucleotide folding and G-quadruplex topology. Molecular modelling on each quadruplex cavity was conducted and accessibility by $HO^{\bullet}$ radicals to these cavities is

described herein and supports the potential role of G-rich tetrads acting as protective sinks (oxidant traps) against chromosomal oxidative damage.[24–30]

Materials and Methods

pUC19 plasmid DNA amplification and manipulation

The pUC19 vector (N3041L, 1,000 μg/ml), restriction enzymes; Nt.BspQI (R0644S, 10,000 U/ml) and HindIII (R0104S, 20,000 U /ml), Bovine Serum Albumen (BSA) (B9001S, 10 mg/ml) and buffers; NEBuffer 3.1 (B7203S, 10 X) and NEBuffer 2 (B7202S, 10 X) were purchased from New England Biolabs (NEB). The pUC19 vector (2686 bp) was amplified to a working concentration employing *E. coli* (MAX efficiency DH5α competent cells, Invitrogen, 8258-012) using an LB ampicillin resistant media protocol. The DNA obtained was extracted and further purified using a NucleoBond Xtra Midi Plus EF kit (Macherey-Nagel, 740422.10). Triplicate DNA quantification was carried out using the NanoDrop (ND-1000) spectrophotometer. The procedure was scaled up in order to generate >300 μg of superhelical, nicked, and linear pUC19 for deoxynucleoside lesion experiments using Nt.BspQI or HindIII endonucleases (1 μl, 10,000 U/ml) where required. Restriction endonuclease experiments were performed by incubating 400 ng of supercoiled pUC19 and bovine serum albumen (0.2 μl, 100 X) with Nt.BspQI or HindIII endonucleases (1 μL, 10,000 U/ml). 1 μl of the respective restriction enzymes (10,000 U/ml), and 2 μl (10 X) of NEBuffer 3.1 (Nt.BspQI) or NEBuffer 2 (HindIII) were added to the digestion reaction and incubated for 2 hours at 37 °C (HindIII) or 50 °C (Nt.BspQI). Reactions were repeated to generate sufficient stocks of nicked and linear pUC19 for subsequent experiments. Nicked and linearised dsDNA were then purified from the enzymatic reaction using QIAquick PCR purification (QIAGEN), eluted in pure water, and quantified using the NanoDrop (ND-

1000) spectrophotometer. The conformation of superhelical pUC19 isolated from *E. coli*, along with enzymatically transformed (nicked and linear) pUC19 dsDNA, were verified by taking an aliquot from each stock and run on gel electrophoresis containing 6x loading dye (Fermentas), with 10 mM Tris-HCl (pH 7.6), 0.03% bromophenol blue, 0.03% xylene cyanol, 60% glycerol and 60 mM EDTA. The samples were loaded onto an agarose gel (1.2%) and electrophoresis was completed at 50 V for 30 minutes and increased to 70 V for 50 minutes using a wide mini-sub cell (BioRad) in 1x TAE buffer (Millipore).

Solid phase oligonucleotide synthesis and characterisation

The syntheses of d(TGGGGT), d(TTGGGTTAGGGTTAGGGTTAGGGA) and d(AGGGTTAGGGTTAGGGTTAGGG) were performed with a DNA synthesizer using solid phase β-cyanoethyl phosphoramidite chemistry at 15 μmol scale. The oligomers were detached from the support and deprotected by treatment with concentrated aqueous ammonia at 328 K for 12 h. The combined filtrates and washings were concentrated under reduced pressure, redissolved in H_2O, analyzed and purified by high-performance liquid chromatography (HPLC) on a Nucleogel SAX column (Macherey–Nagel, 1000-8/46); using buffer A: 20 mM KH_2PO_4/K_2HPO_4 aqueous solution (pH 7.0), containing 20% (v/v) CH_3CN; buffer B: 1 M KCl, 20 mM KH_2PO_4/K_2HPO_4 aqueous solution (pH 7.0), containing 20% (v/v) CH_3CN; a linear gradient from 0 to 100% B for 30 min and flow rate 1 mL/min were used. The fractions of the oligomers were collected and successively desalted by Sep-pak cartridges (C-18). The isolated oligomers proved to be > 98% pure by NMR. The G-quadruplexes formed by d(TGGGGT) and d(TTGGGTTAGGGTTAGGGTTAGGGA) were prepared dissolving the oligonucleotides in 10 mM KH_2PO_4 buffer containing 70 mM $KClO_4$ (pH

7.0)(~35 OD and ~50 OD, respectively), while d(AGGGTTAGGGTTAGGGTTAGGG) was dissolved in 10 mM NaH_2PO_4 buffer containing 70 mM $NaClO_4$ (pH 7.0) (~50 OD). Different buffers are required to avoid conformational heterogeneity. [23,31,32] All the samples were heated for 10 min at 80 °C and then slowly cooled down to room temperature. The 1D ^{1}H-NMR spectra showed that d(TGGGGT) and d(TTGGGTTAGGGTTAGGGTTAGGGA) were able to form a single well-defined hydrogen-bonded structure in solution, whereas d(AGGGTTAGGGTTAGGGTTAGGG) was in equilibrium between the folded (G-quadruplex) and the non-folded form (Figure S1).

γ-Radiolysis experiments and enzymatic digestion of nucleosides

Materials

8-Oxo-7,8-dihydro-2'-deoxyadenosine (8-oxo-dA) and 8-oxo-7,8-dihydro-2'-deoxyguanosine (8-oxo-dG) were purchased from Berry & Associates Inc. (Dexter, USA). Isotopic labelled lesions were prepared as described elsewhere.[12] All salts and solvents, Nuclease P1 from Penicillium citrinum, phosphodiesterase II, phosphodiesterase I from Crotalus Adamanteus venom, DNase I, DNase II, alkaline phosphatase from bovine intestinal mucosa, erythro-9-(2-hydroxy-3-nonyl)adenine hydrochoride (EHNA), benzonase 99%, deferoxamine mesylate salt, BHT and pentostatin, were obtained from Sigma (Taufkirchen, Germany and Milan, Italy) while the 3 kDa cut-off filters were purchased from Millipore (Bedford, USA). Distilled and deionized water (ddH_2O) were purified by a Milli-Q system (Millipore, Bedford, USA).

Gamma-Irradiaton Experiments

Preparation of dsDNA samples (SC, OC, L): Each sample of dsDNA (100 μg) was dissolved (200 μl) in double distilled water (ddH_2O) by gently rocking. Next, the solution was placed in a glass vial of 2 ml containing 300 μl glass insert. The solution was flushed with N_2O/O_2 95:5 for 10 min and exposed to gamma rays in a ^{60}Co Gammacell apparatus (dose rate 4.7 Gy/min). The irradiation doses used were 0 and 100 Gy respectively. In every sampling (50 μl) a balloon filled with N_2O/O_2 95:5 mixture was supporting the sample with the necessary amount of gas in order to keep the reaction conditions unaltered. The samples were freeze-dried before subjecting to enzymatic digestion. All irradiation experiments were performed in triplicate at ambient temperature (25 ^{o}C).

Preparation of the ODN samples for experiments with unfolded and folded in G-quadruplex structures: Each sample of ODN was dissolved in ddH_2O (non-folded ODN) or the appropriate phosphate buffer containing perchlorate anions (folded ODN) by gently rocking in order to have concentrations of ~80 OD / 1 ml for the ODN1 and ODN2 or ~60 OD / 1 ml for the ODN3, respectively. In a typical experiment, a 40 μl solution (in case of ODN3 60 μl were used) was placed in a glass vial of 2 ml containing 100 μl glass insert. The solution was flushed with N_2O for 10 min and exposed to gamma rays in a ^{60}Co Gammacell apparatus (dose rate 4.7 Gy/min). The irradiation dose was increased from 0 to 20, 40, and 60 Gy, respectively. In every sampling (10 μl; or 15 μl in case of ODN3) a balloon filled with N_2O was supporting the sample with the necessary amount of gas in order to keep the reaction conditions unaltered. After irradiation, the samples containing buffers and salts were transferred in a microspin filters (3 kDa), ddH_2O was added and then desalinated by centrifugation at 14000 *g* (4 ^{o}C) for 20 minutes. Subsequently, the samples were freeze-dried and

digested enzymatically. All the irradiation experiments were performed in triplicate at ambient temperature (25 ^{o}C).

Enzymatic Digestion

Digestion of the dsDNA samples (SC, OC, L): The freeze-dried samples from the experiments with the dsDNA were digested according to a protocol described previously.[12] In a typical experiment, 25 μg dsDNA were dissolved in 50 μL of Ar flushed 10 mM Tris-HCl buffer pH 7.9 containing 10 mM $MgCl_2$, 50 mM NaCl, 0.2 mM pentostatin, 5 μM BHT and 3 mM deferoxamine and the isotopic analytes that were used as internal standards. Next, 1.5 U of benzonase (in 20 mM Tris HCl pH 8.0, 2 mM $MgCl_2$ and 20 mM NaCl), 2 mU phosphodiesterase I, 1.5 U DNAse I, 1 mU of PDE II and 1 U of alkaline phosphatase were added and the mixture was incubated at 37 °C. After 21h, 17 μL of Ar flushed buffer containing 0.3 M AcONa and 10 mM $ZnCl_2$ (pH 5.6) were added along with 0.3 U of Nuclease P1 (in 30 mM AcONa pH 5.3, 5 mM $ZnCl_2$ and 50 mM NaCl), 2 mU phosphodiesterase II and 62 mU of DNAse II and the mixture was further incubated at 37 °C for other 21 h. Next, 10 μL of 0.5 M Tris HCl pH 8.9 were added and the incubation continued for other 2 h, before quenching with 1% formic acid solution (pH 7.0). The digestion mixture was placed in a microspin filter (3kDa) and the enzymes were filtered off by centrifugation at 14000 *g* (4 ^{o}C) for 20 minutes. Subsequently, the filtrate was freeze-dried before HPLC analysis, clean-up and enrichment.

Digestion of the oligonucleotide samples (ODN1 (mutTel24), ODN2 (Tel22), ODN3 (TG4T)): The freeze-dried samples from the experiments with the three different ODNs were digested according to a protocol based on Nuclease P1 reported previously in the

literature[33] but in absence of oxygen and in presence of antioxidants and a chelator.[12] It is worth mentioning that the enzyme benzonase alone was incapable of reaching complete digestion of the oligos used (HPLC traces of peaks probably dimers were found upon first trials; benzonase is known for this action[34]). In particular, 0.5 OD (~25 μg) of ODN were dissolved in 10 μl of Ar flushed buffer containing 0.3 M AcONa (pH 5.6), 10 mM $ZnCl_2$, 3 mM deferoxamine mesylate, 1 mM EHNA and the isotopic analytes that were used as internal standards. Next, 2 U of Nuclease P1 (in 30 mM AcONa pH 5.3, 5 mM $ZnCl_2$ and 50 mM NaCl) and 2.5 mU phosphodiesterase II were added, and the mixture was incubated at 37 °C for 48 h under inert atmosphere before the addition of 10 μl of 0.5 M Tris-HCl buffer (pH 8.9; also flushed with Ar) and 2 U of alkaline phosphatase together with 2.5 mU of phosphodiesterase I. The mixture was incubated for an extra 2 h before quenching with 1% formic acid. The digestion mixture was transferred in a microspin filter (3 kDa) and centrifuged at ~14000 *g* for 20 min (4 °C) for the removal of the enzymes. The filtrate was freeze-dried before HPLC analysis, clean-up and enrichment.

Stable isotope LC-MS/MS analysis and purine lesion quantification

The quantification of the lesion (in lesions / 10^6 normal nucleosides units) in the enzymatically digested samples (spiked with the internal standards prior to digestion) were based on the parallel quantification of the unmodified nucleosides after HPLC clean-up and sample enrichment (according to their absorption against their response calibration curves, at 260 nm), and the quantification of the single lesions by stable isotope dilution LC-MS/MS analysis (LC, Perkin Elmer Inc., USA; triple quadrupole MS/MS, Q-Trap 4000, AB Sciex Inc., Canada). The enzyme free samples were injected into the HPLC-UV system and the peaks resolved on a 4.6 mm x 150 mm Luna C18 (2)

100 Å column (5 µm particle size, Phenomenex). In each analysis, the unmodified nuclosides were quantified, the fractions containing the lesions were collected (the time windows were identified by injection of a pure standard of a lesions mixture), pooled and then freeze-dried. Next, the samples were dissolved in a constant volume of double distilled H_2O and subjected to LC-MS/MS analysis (Multiple Reaction Monitoring mode). The analytes resolved on a 2 mm x 150 mm Luna C18 (2) 100 Å column (3 µm particle size, Phenomenex) and the values of the lesions calculated against their response calibration curves.[12] In this study, folded ODNs were examined in phosphate buffered solution containing perchlorate anions, while non-folded ODNs were examined in unbuffered solution (dd H_2O).

Structural analysis of G-quadruplex structures

Table S1 gathers solvent-accessible surface areas (SASA) for ODN1 (mutTel24), ODN2 (Tel22), and ODN3 (TG4T) structures, computed using the POPS program[34] at atomic level (server: http://mathbio.nimr.mrc.ac.uk/wiki/POPS[36]) with a radius probe of 1.33 Å. SASA values restricted to guanine-only were also estimated using the molecular modeling software VMD Version 1.9.1.[37] We note that very similar values and SASA ranking are obtained with VMD (respectively 4122.96, 3912.74, 4470.87 and 6536.25 $Å^2$). The area equation is defined by a product Π of terms that estimate the reduction of SASA of atom *i* by the overlap with its neighbours *j*: $\Pi_{i=1}^{N}$ [1 - (p_i p_{ij} $b_{ij}(r_{ij})$ / S_i)][38]. *i* is the atom for which the POPS* area is computed, *j* is any of N neighbour atoms. p_i is an atom type specific SASA parameter. p_{ij} is a sphere overlap parameter depending on the degree of bonding between *i* and *j* (1-2, 1-3, 1-4, 1-(>4)). b_{ij} is a geometric construct based on the radii and distance (r_{ij}) of *i* and *j*. S_i is the SASA of the free atom *i* (no neighbours). The atom specific parameters (radii, SASAs) are listed

in the Parameters files for the atoms of all standard PDB residues, followed by the connectivity parameters (p_{ij}, b_{ij}) and the solvent radius for water. Surface and volume for the cavities displayed in Figure 3 were computed using the CASTp (Computed Atlas of Surface Topography of proteins[39]). For 1KF1 (Figure 3c), the four cavities occupy a total surface of 501.5 $Å^2$, for a corresponding volume of 673.8 $Å^3$. These calculations were also performed using a radius probe of 1.33 Å.

Results and Discussion

Quantification of purine lesions in dsDNA conformers

In this study we enzymatically manipulated negatively charged supercoiled (SC) pUC19 plasmid dsDNA, a 2686 bp vector containing 51% G·C, to obtain the open circular (OC), and linear (L) tertiary forms. Total plasmid dsDNA pUC19 vector was isolated from an overnight LB ampicillin resistant *E. coli* media and exploited in its natural SC form. SCDNA was transformed using type II restriction endonucleases Nt.BspQI, a nicking enzyme that induces one single strand break on pUC19, and HindIII, a double strand cleaving enzyme with one recognition site on pUC19, to generate OC and L forms (Figure 1a-c), respectively. Nicked and linear dsDNA conformers were purified from the enzymatic reaction using a standard nucleic acid purification protocol (Qiagen QIAquick PCR Purification) and eluted in pure water before being quantified on the NanoDrop spectrophotometer. To confirm transformation and purity, the three conformers SC, OC and L dsDNA were subject to gel electrophoresis (Figure 1c). Aqueous DNA solutions of each conformer (150 µg/300 µL) were then γ-irradiated using a ^{60}Co source (4.7 Gy/min). It is known that radiolysis of neutral water leads to reactive species of hydrated electrons (e_{aq}^-, 0.27), hydrogen atoms ($H^•$, 0.062) and hydroxyl radicals ($HO^•$, 0.28) where the values in parentheses represent the radiation

chemical yields (G) in units of μmol J^{-1}.[40] In a N_2O(95%)/O_2(5%)-saturated solution (~0.02 M of N_2O and 6.7x10^{-5} M of O_2), e_{aq}^- are transformed into $HO^\bullet$ through reaction with N_2O (k = 9.1 x 10^9 M^{-1} s^{-1}), whereas $H^\bullet$ are efficiently converted into $O_2^{\bullet-}$ (k = 2 × 10^{10} M^{-1} s^{-1}, pK_a($HOO^\bullet$) = 4.8).[40] Since $O_2^{\bullet-}$ does not react with DNA, these are appropriate biomimetic conditions for studying the reaction of $HO^\bullet$ radicals with DNA in the presence of oxygen.[12]

Figure 1 here

The levels of lesions produced were determined prior to irradiation by enzymatic digestion in conditions that avoid oxidation artefacts. Stable isotope dilution LC-MS/MS analysis was employed in the enzymatically digested samples, previously spiked with the internal standard. [12,13] Figure 2 (blue colour) shows the average of 3 independent measurements. The purine lesions followed the order: 8-oxo-dG >> 8-oxo-dA >> 5′,8-cdG ≈ 5′,8-cdA, with the SC conformation being more resistant to autoxidation. The quantities of lesions in SC form are more than an order of magnitude lower than the corresponding values observed in commercial calf thymus dsDNA[12,13] indicating the high quality of plasmid production and purification. Initially, the radiation dose was changed from 0 to 50, and 100 Gy, and the 8-oxo-dG and 8-oxo-dA lesions increased linearly as previously observed in calf thymus dsDNA,[12] whereas 5′,8-cdG and 5′,8-cdA remained essentially unchanged. Due to the limited amount of stating materials, we decided to run only the experiment at 100 Gy in triplicate. Interestingly, the levels of (5'*R*)-5′,8-cdG, (5'*R*)-5′,8-cdA, and (5'*S*)-5′,8-cdA did not increase with respect to background levels after 100 Gy in all three dsDNA

conformations (Figure 2), whereas only slight increases were observed for 5'*S*-cdG in OC and L forms.

Figure 2 here

The overall 8-oxo lesion formation, regardless of topology, followed 8-oxo-dG >> 8-oxo-dA (Figure 2). DNA damage between tertiary dsDNA forms are stark and in the order L > OC >> SC indicating significantly higher damage toward extended, or unwound, B-DNA topologies. Indeed, 8-oxo-dG levels rose from 13.9 for SC to 140.7 and 180.2 lesions for OC and L forms, respectively. Differences in 8-oxo-dA levels among tertiary forms were found to be smaller but noteworthy, i.e. a rise from 0.2 for SC to ~8.0 for OC and L was observed. We suggest the 8-oxo lesions are generated by addition of $HO^{\bullet}$ onto C8 position and the higher yield of 8-oxo-dG formation compared to 8-oxo-dA reflects additional mechanisms such as one-electron oxidation in dsDNA that occurs via hole transfer and water assistance and/or the formation of 8-oxo-dG through the intramolecular tandem damage involving base-derived peroxyl radicals. [2,10,42] Overall, it is noteworthy how supercoiled DNA structure attenuates solution-borne $HO^{\bullet}$ free radical damage, with 8-oxo-dG and 8-oxo-dA levels increasing ≥10 fold within both circular and linear conformers. Within the three tertiary forms, the very low levels recorded for purine 5′,8-cyclo-2′-deoxynucleoside lesions are in agreement with the low efficiency of such radiation-induced lesions in cellular DNA.[11] On the other hand, these lesions are harmful since they accumulate with aging in a tissue specific manner (liver > kidney > brain)[33,41] suggesting that DNA repair mechanisms are inadequate to effectively deal with these lesions.[16]

Quantification of purine lesions in G-quadruplex nucleic acid sequences

Purine lesion formation within G-quadruplex folded (and non-folded) tetrads of TG4T, Tel22, and mutTel24 (Figure 3) were next identified under γ-irradiation conditions. In order to study the impact of G-quadruplex folding on the formation of four 5',8-cyclopurines (5',8-cPus) and two 8-oxo purine lesions, all three sequences were examined in folded (buffered) and unfolded (unbuffered) solution. All sequences were verified by NMR experiments to adapt the G-quadruplex conformation in the presence of phosphate buffers containing perchlorates; results also showed that in the absence of buffer and salts, sequences were unfolded and existed as single strands. The use of the chloride anion, commonly used in G-quadruplex structural experiments as a counter ion, was obligatorily exchanged with perchloride due to its incompatibility with gamma irradiation conditions (see Materials and Methods section). NMR results show the use of the buffers and salts forced the TG4T and mutTel24 to self-organize, up to 90% into quadruplex structures with guanine residues in tetrad configuration. Nevertheless, Tel22 was unable to exceed 50% in total G-quadruplex folding and so provided an elegant insight into tetrad folding effects on purine lesion formation under direct comparison with mutTel24.

Figure 3 here

Aqueous solutions of oligodeoxynucleotides **(**ODNs) were prepared and irradiated with 0 Gy, 20 Gy, 40 Gy and 60 Gy in a ^{60}Co Gamma Cell apparatus (4.7 Gy/min). In order to generate detectible differences in levels of cyclopurine lesions, experiments were conducted under saturated N_2O conditions before purification, enzymatic digestion, and enrichment prior to stable isotope dilution LC-MS/MS

analysis. Purine lesion formation increases linearly with radiation intensity rising from 0 Gy to 60 Gy (Figures S2 and S3). The results from the quantification of the four 5',8-cPus and two 8-oxo purines are summarised in Table 1 including maximum standard errors in the range from 0 to 60 Gy of irradiation. In agreement with literature reports, the major lesion formed in all cases was 8-oxo-dG.[4] Of particular significance, we found self-organization of guanines in G-quadruplex tetrads produced ~3 and ~4 fold increases in 8-oxo-dG yields (entries 1 and 3) and from ~2 to ~4 fold enhancement in 5'*R*-cdG (entries 7 and 9), while 5'*S*-cdG yields remained almost constant (entries 4-6). The incomplete (50%) self-organization of the Tel22 in presence of phosphate buffer and perchlorate salts was found to play a dramatic role in the formation of guanine lesions; yields were kept at essentially the same levels as those obtained from the unfolded experiments (entries 2, 5 and 8). Additionally, dA nucleosides (Tel22 and mutTel24 only) participating in G-quadruplex loop and termini were also influenced by quadruplex folding. Particularly, the formation of 5'*R*- and 5'*S*-cdA and 8-oxo-dA increased by ~2 fold in both mutTel24 and Tel22 (entries 10, 11, 13, 14, 16 and 17) in their folded conformation. Taken together, data here indicates G-quadruplex folded sequences are significantly more susceptible to purine $HO^{\bullet}$ oxidation. Guanine lesions follow 8-oxo-dG >> 5'*S*-cdG ≥ 5'*R*-cdG for unfolded sequences, while for folded G-quadruplex this order changes to 8-oxo-dG >> 5'*R*-cdG ≥ 5'*S*-cdG.

Table 1 here (note this is a new table)

Given their potential role in acting as protective sinks against chromosomal oxidative damage,[27–29] G-quadruplex architectures have been extensively examined for their charge conduction properties. In particular, adjacent guanines in G-quartets

appear to be very effective nucleobases for excess electron transfer.[30] Our results clearly demonstrate that self-organisation of G-rich sequences gives rise to higher numbers of oxidative purine lesions. In order to shed further light on this axiom, solvent cavities in each sequence (TG4T, Tel22 and muTel24) were examined—at the hydroxide anion radius (1.33 Å)—and are shown in Figure 3 (wireframe, teal). The human telomere sequence d[$AG_3(TTAGGG)_3$] (Tel22) is known to form an antiparallel 'basket' structure in that Tel22 adopts the same folding topology within phosphate buffered perchlorate. Hydroxyl radical solvent accessible surface areas (SASA) differ widely within the cavities of both parallel and antiparallel Tel22; the antiparallel (143D) tetrad has three small cavities—occupying 155.9 $Å^2$ in total (157.6 $Å^3$)—that occupy three quadrants of the quadruplex base at T5/G3/G9, G4/A2/G10, and G8/G9/G10/G11 interfaces (Figure 3e). Modification of the Tel22 sequence by adding 5′ and 3′ extensions such as TT/TA and A/TT, respectively, are known to stabilise hybrid parallel and antiparallel topologies consisting of two lateral loops and one side-chain reversal loop.[23] In the mutTel24 hybrid-1 state d[$TTG_3(TTAGGG)_3A$] (2GKU), the 5′ loop is in the reversed configuration giving rise to the (3 + 1) configuration (Figure 3a) and NMR results confirm the structure is indeed stabilised relative to Tel22 (Figure S1). A single, large volume, hydroxyl radical cavity (172.8 $Å^2$, 233.2 $Å^3$) was identified at the 5′ end (Figure 3f) in close proximity to G1 – G4 residues and their flanking thymine (T1 – T4) and adenine (A1) parallel loop residues. The final G-quadruplex sequence examined in this study, d$[TGGGGT]_4$ (1S47),[20] is the tetra-guanine (parallel-stranded) quadruplex and contains the largest hydroxyl solvent cavity space of all three ODNs examined (1545.5 $Å^2$, 1159.3 $Å^3$). In this structure, four cavities exist along the interface between each parallel strand with additional available cavity space between metal ions within the tetrad core (Figure 3d).

Conclusions

In summary, this work has identified how hydroxyl radical-induced purine oxidation is attenuated by tertiary helical structure and G-quadruplex folding. While it is interesting to note the larger hydroxyl cavity space and total molecular surface area available within mutTel24 and TG4T sequences compared to Tel22 (4587 $Å^2$, mutTel24; 4279 $Å^2$, Tel22; 7142 $Å^2$, TG4T), this analysis alone does not account for increased purine lesion formation within folded G-quadruplex structures. This work suggests, therefore, it is likely purine damage occurs in proportion to specific quadruplex topology—indicating a potential role in their action as oxidant traps to protect against chromosomal DNA damage—independent of guanine content; this point is exemplified by comparing numbers of lesions generated in stabilised (mutTel24) and non-stable (Tel22) tetrads, and also 8-oxo-dG lesions produced by mutTel24 (12 G base) and TG4T (16 G base) quadruplexes. With regard to lesion formation with dsDNA conformers, results here indicate greater damage toward extended, or unwound, B-DNA topology as the overall oxidation trend follows linear conformation > open circular >> supercoiled. To our knowledge this is the first evidence reporting hydroxyl radical-induced nucleic acid damage is attenuated by tertiary helical DNA structure. One consideration is solvent accessibility to dsDNA conformers; if superhelical pUC19 DNA has significantly lower solvent—and by extension $HO^{\bullet}$ radical—accessibility compared with open circular and linear isoforms, the ensuing production of oxidative purine lesions would naturally be lower. Furthermore, it is noteworthy how supercoiled DNA structure attenuates hydroxyl free radical damage with 8-oxo-dG and 8-oxo-dA levels ≥10 fold within both circular and linear conformers. Of further significance is the comparison of dsDNA oxidation results obtained here with recent observations on γ-irradiation damage distribution to single stranded (ss) and double stranded (ds) calf thymus DNA; $HO^{\bullet}$

insult (under identical N_2O:O_2 conditions) showed *ca*. 2 times higher levels of 8-oxo-dG and 8-oxo-dA within ssDNA as compared with dsDNA[12] that shows, in direct contrast to unfolded G-quadruplex structures, greater damage toward non-hybridised purine nucleosides.

Acknowledgements

This work was supported by the Irish Research Council [GOIPG/2013/937 and GOIPG/2013/826], EU COST Action CM1201: Biomimetic Radical Chemistry, Marie Curie Intra-European Fellowship [CYCLOGUO298555], Italian Association for Cancer Research (AIRC) [IG-14150], GGET/SIEMENS Program «Establishing a Multidisciplinary and Effective Innovation and Entrepreneurship Hub», and the Marie Skłodowska-Curie European Training Network (ETN) ClickGene: Click Chemistry for Future Gene Therapies to Benefit Citizens, Researchers and Industry [H2020-MSCA-ETN-2014-642023].

References

[1] Geacintov NE, Shafirovich V. Reaction of Small Reactive Species with DNA. In: Chatgilialoglu C, Studer A (eds). Encyclopedia of Radicals In Chemistry, Biology and Materials. Chichester: Wiley, 2012. pp 1283–1317.

[2] Cadet J, Douki T, Gasparutto D, Ravanat J-L, Wagner JR. Oxidatively Generated Nucleobase Modifications in Isolated and Cellular DNA. In: Chatgilialoglu C, Studer A (eds). Encyclopedia of Radicals In Chemistry, Biology and Materials. Chichester: Wiley, 2012. pp 1319–1344.

[3] Gimisis T, Chatgilialoglu C. Oxidatively Formed Sugar Radicals in Nucleic Acids. In: Chatgilialoglu C, Studer A (eds). Encyclopedia of Radicals In Chemistry, Biology and Materials. Chichester: Wiley, 2012. pp 1345–1370.

[4] Chatgilialoglu C, Ferreri C, Terzidis MA. Purine 5',8-cyclonucleoside lesions: chemistry and biology. Chem Soc Rev 2011;40:1368–1382.

[5] Kuraoka I, Bender C, Romieu A, Cadet J, Wood RD, Lindahl T. Removal of oxygen free-radical-induced 5',8-purine cyclodeoxynucleosides from DNA by the nucleotide excision-repair pathway in human cells. Proc Natl Acad Sci USA 2000;97:3832–3837.

[6] Kropachev K, Ding S, Terzidis MA, Masi A, Liu Z, Cai Y, Kolbanovskiy M, Chatgilialoglu C, Broyde S, Geacintov NE, Shafirovich V. Structural basis for the recognition of diastereomeric 5',8-cyclo-2'-deoxypurine lesions by the human nucleotide excision repair system. Nucleic Acid Res 2014;42:5020–5032.

[7] Cadet J, Douki T, Ravanat J-L. Oxidatively Generated Damage to the Guanine Moiety of DNA: Mechanistic Aspects and Formation in Cells. Acc Chem Res 2008;41:1075–1083.

[8] Chatgilialoglu C, Krokidis MG, Papadopoulos K, Terzidis MA. Purine 5',8-cyclo-2'-deoxynucleoside lesions in irradiated DNA. Radiat Phys Chem 2016; in press.

[9] Battino R, Rettich TR, Tominaga T. Solubility of oxygen and ozone in liquids. J Phys Chem Ref Data 1983;12:163–178.

[10] Bergeron F, Auvré F, Radicella JP, Ravanat J-L. HO* radicals induce an unexpected high proportion of tandem base lesions refractory to repair by DNA glycosylases. Proc Natl Acad Sci USA 2010;107:5528–5533.

[11] Belmadoui N, Boussicault F, Guerra M, Ravanat J-L, Chatgilialoglu C, Cadet J. Radiation-induced formation of purine 5′,8-cyclonucleosides in isolated and cellular DNA: high stereospecificity and modulating effect of oxygen. Org Biomol Chem 2010;8:3211–3219.

[12] Terzidis MA, Ferreri C, Chatgilialoglu C. Radiation-induced formation of purine lesions in single and double stranded DNA: revised quantification. Front Chem 2015;3:article 18.

[13] Terzidis MA, Chatgilialoglu C. An ameliorative protocol for the quantification of purine 5′,8-cyclo-2′-deoxynucleosides in oxidized DNA. Front Chem 2015;3:article 47.

[14] Liu LF, Wang JC. Supercoiling of the DNA template during transcription. Proc Natl Acad Sci USA 1987;84:7024–7027.

[15] Sinden RR. The helix turns at 60: writhing free in chromosomes. Nat Struct Mol Biol 2013;20:251–253.

[16] Cai Y, Kropachev K, Terzidis MA, Masi A, Chatgilialoglu C, Shafirovich V, Geacintov NE, Broyde S. Differences in the access of lesions to the nucleotide excision repair machinery in nucleosomes. Biochemistry 2015;54:4181–4185.

[17] Lipps HJ, Rhodes D. G-quadruplex structures: in vivo evidence and function. Trends Cell Biol 2009;19:414–422.

[18] Hsu SD, Varnai P, Bugaut A, Reszka AP. A G-rich sequence within the c-kit oncogene promoter forms a parallel G-quadruplex having asymmetric G-tetrad dynamics. J Am Chem Soc 2011;131:13399–13409.

[19] Biffi G, Tannahill D, McCafferty J, Balasubramanian S. Quantitative visualization of DNA G-quadruplex structures in human cells. Nat Chem 2013;5:182–186.

[20] Cáceres C, Wright G, Gouyette C, Parkinson G, Subirana JA. A thymine tetrad in d(TGGGGT) quadruplexes stabilized with TI+/Na+ ions. Nucleic Acids Res 2004;32:1097–1102.

[21] Wang Y, Patel DJ. Solution structure of the human telomeric repeat d[AG3(T2AG3)3] G-tetraplex. Structure 1993;1:263–182.

[22] Parkinson GN, Lee MP, Neidle S. Crystal structure of parallel quadruplexes from human telomeric DNA. Nature 2002;20:876–880.

[23] Luu KN, Phan AT, Kuryavyi V, Lacroix L, Patel DJ. Structure of the human telomere in K+ solution: an intramolecular (3 + 1) G-quadruplex scaffold. J Am Chem Soc 2006;2:9963–9970.

[24] Núñez ME, Hall DB, Barton JK. Long-range oxidative damage to DNA: Effects of distance and sequence. Chem. Biol. 1999;6:85–97.

[25] Delaney S, Barton JK. Charge transport in DNA duplex/quadruplex conjugates. Biochemistry 2003;42:14159–14165.

[26] Friedman KA, Heller A. On the non-uniform distribution of guanine in introns of human genes: possible protection of exons against oxidation by proximal intron poly-G sequences. J Phys Chem B 2001;105:11859–11865.

[27] Friedman KA, Heller A. Guanosine distribution and oxidation resistance in eight eukaryotic genomes. J Am Chem Soc 2004;126:2368–2371.

[28] Das RS, Samaraweera M, Morton M, Gascón JA, Basu AK. Stability of N-glycosidic bond of (5′ S)-8,5′-cyclo-2′-deoxyguanosine. Chem Res Toxicol 2012;25:2451–2461.

[29] Huang YC, Cheng AKH, Yu H-Z, Sen D. Charge conduction properties of a parallel-stranded DNA G-quadruplex: implications for chromosomal oxidative damage. Biochemistry 2009;48:6794–6804.

[30] De Champdoré M, De Napoli L, Montesarchio D, Piccialli G, Caminal C, Mulazzani QG, Navacchia ML, Chatgilialoglu C. Excess electron transfer in G-quadruplex. Chem. Commun. 2004;1756–1757.

[31] Cosconati S, Marinelli L, Trotta R, Virno A, Mayol L, Novellino E, Olson AJ, Randazzo A. Tandem application of virtual screening and NMR experiments in the discovery of brand new DNA quadruplex groove binders. J Am Chem Soc 2009;131:16336–16337.

[32] Lim KW, Ng VCM, Martin-Pintado N, Heddi B, Phan AT. Structure of the human telomere in Na+ solution: an antiparallel (2+2) G-quadruplex scaffold reveals additional diversity. Nucleic Acids Res. 2013;41:10556–10562.

[33] Wang J, Yuan B, Guerrero C, Bahde R, Gupta SW. Quantification of oxidative DNA lesions in tissues of long- evans cinnamon rats by capillary high-performance liquid chromatography-tandem mass spectrometry coupled with stable isotope-dilution method. Anal Chem 2011;83:2201–2209.

[34] Liao Q, Chiu NHL, Shen C, Chen Y, Vouros P. Investigation of enzymatic behavior of benzonase/alkaline phosphatase in the digestion of oligonucleotides and DNA by ESI-LC/MS. Anal Chem 2007;79:1907–1917.

[35] Cavallo L, Kleinjung J, Fraternali F. POPS: a fast algorithm for solvent accessible surface areas at atomic and residue level. Nucleic Acids Res 2003;31:3364–3366.

[36] Kleinjung J, Fraternali F. POPSCOMP: an automated interaction analysis of biomolecular complexes. Nucleic Acids Res 2005;33:342–346.

[37] Humphrey W, Dalke A, Schulten K. VMD: visual molecular dynamics. J Mol Graph 1996;14:27–28.

[38] Hasel W, Hendrickson TF, Still WC. A rapid approximation to the solvent accessible surface areas of atoms. Tetrahedron Comput Methodol 1988;1:103–116.

[39] Dundas J, Ouyang Z, Tseng J, Binkowski A, Turpaz Y, Liang J. CASTp: Computed atlas of surface topography of proteins with structural and topographical mapping of functionally annotated residues. Nucleic Acids Res 2006;34:116–118.

[40] Buxton GV, Greenstock CL, Helman WP, Ross AB. Critical review of rate constants for reactions of hydrated electrons, hydrogen atoms and hydroxyl radicals (*OH/*O−) in aqueous solution. J Phys Chem Ref Data 1988;17:513–886.

[41] Wang J, Clauson CL, Robbins PD, Niedernhofer LJ, Wang Y. The oxidative DNA lesions 8,5′-cyclopurines accumulate with aging in a tissue-specific manner. Aging Cell 2012;11:714–716.

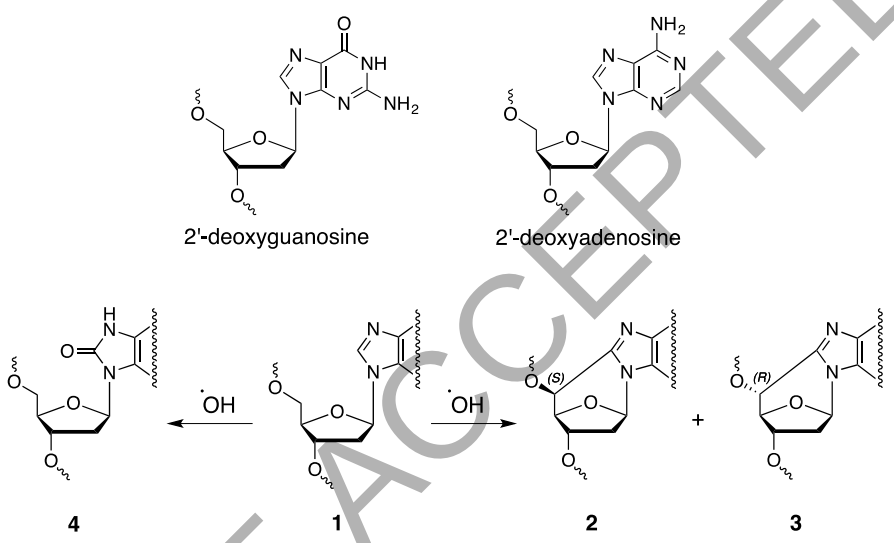

Scheme 1. Purine 2'-deoxynucleosides (**1**) react with hydroxyl radicals (HO•) yielding the diastereomeric (5'*S*)- 5',8- cyclo (**2**) and (5'*R*)-5',8- cyclo (**3**) derivatives along with 8-oxo-dG and 8-oxo-dA lesions (**4**).

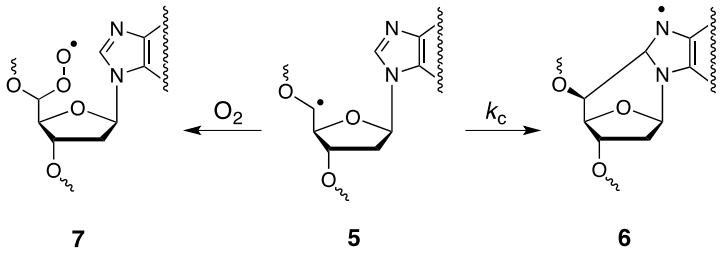

Scheme 2. Partition of C5′ radical **5** between cyclisation reaction to give **6** and molecular oxygen addition to give **7**.

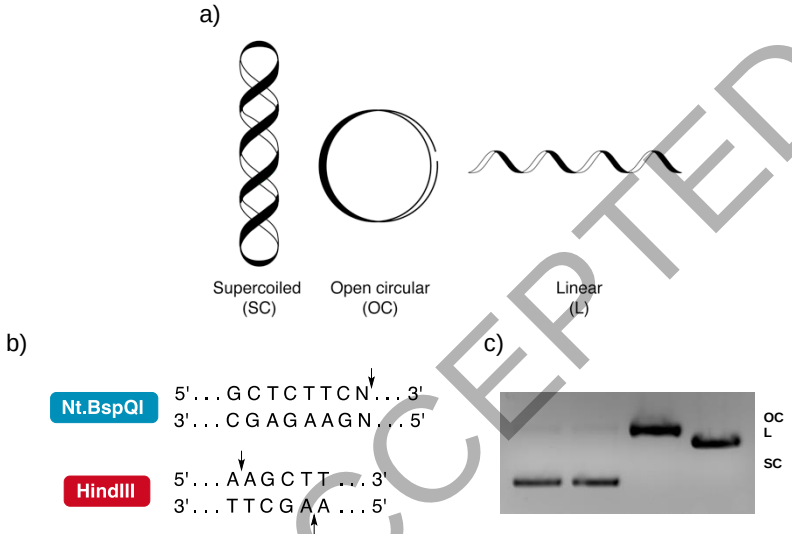

Figure 1. a) Supercoiled (SC), relaxed (OC), and linear (L) pUC19 tertiary dsDNA structures employed. b) Site-specific recognition sequences of the nicking endonuclease Nt.BspQI and type II restriction endonuclease HindIII. c) Agarose gel electrophoresis of pUC19 (400 ng) tertiary structures; lane 1. superhelical pUC19; lane 2. superhelical pUC19 + BSA; lane 3. superhelical pUC19 + Nt.BspQI + BSA; lane 4. superhelical pUC19 + HindIII + BSA.

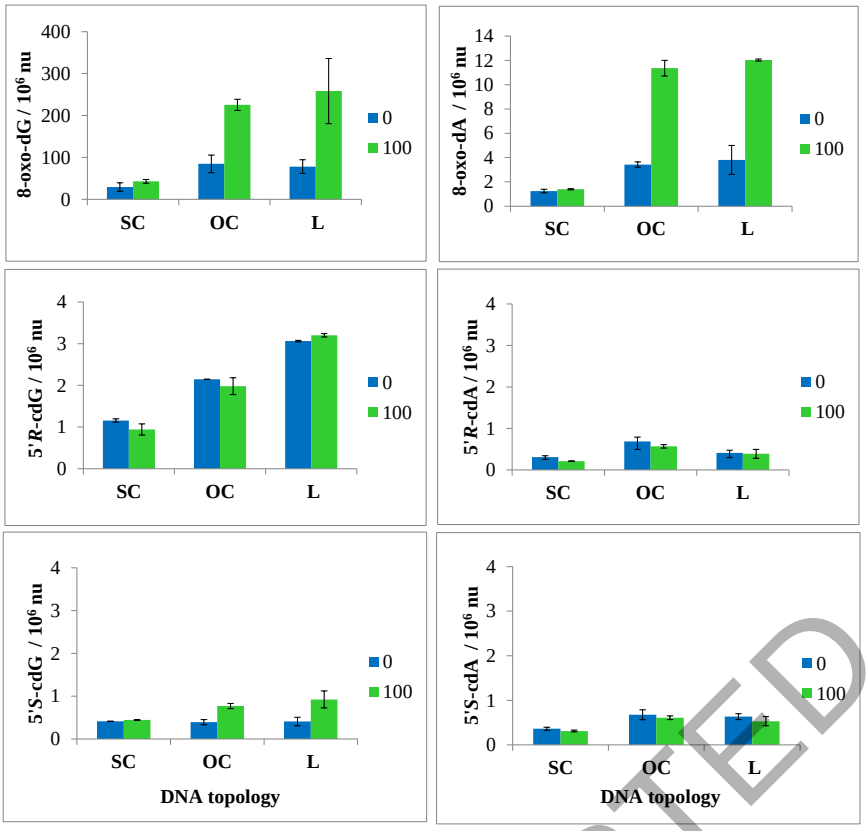

Figure 2. Purine lesions/10^6 Nu for 8-oxo-dG, 5'*R*-cdG, 5'*S*-cdG (left side) and 8-oxo-dA, 5'*R*-cdA, 5'*S*-cdA (right side) in supercoiled (SC), open circular (OC), and linear (L) dsDNA forms; Blue: prior to γ-radiation (0 Gy); Green: exposed to 100 Gy dose in the presence of N_2O(95%)/O_2(5%)-saturated solution. Results from *n*=3 independent experiments.

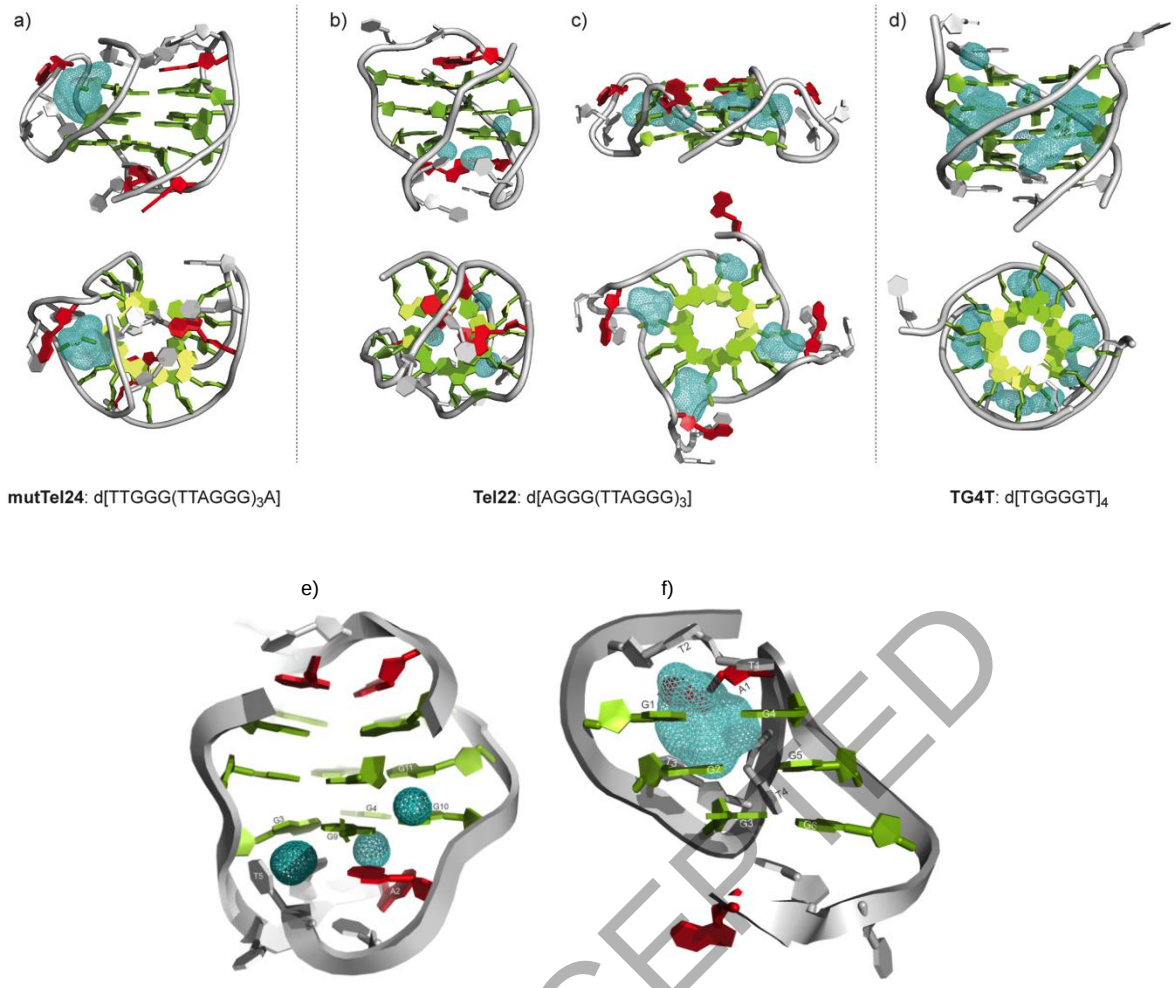

Figure 3. a) Structures of the human telomeric G-quadruplex d[TTGGG(TTAGGG)$_3$A] (mutTel24) (PDB entry 2GKU), b) solution structure of Na^+ stabilised human antiparallel telomeric G-quadruplex d[AGGG(TTAGGG)$_3$] (Tel22) (PDB entry 143D) c) X-ray structures of K^+ stabilised human parallel telomeric G-quadruplex d[AGGG(TTAGGG)$_3$] (Tel22) (PDB entry 1KF1), d) perspective X-ray structures of the thymine flanked G-quartet in Na^+/Tl^+ stabilised d[TGGGGT]$_4$ (TG4T) (PDB entry 1S47). e) Selected residues of Na^+ stabilised human antiparallel telomeric G-quadruplex d[AGGG(TTAGGG)$_3$] (Tel22) (PDB entry 143D), and f) selected residues human telomeric G-quadruplex d[TTGGG(TTAGGG)$_3$A] (mutTel24) (PDB entry 2GKU) (right). DNA backbone (connecting P positions), gray90; colour code for DNA bases: guanine, green; adenine, red; thymine, grey90 (all in cartoon mode). Quadruplex solvent cavities, modelled at the hydroxide anion atomic radius (1.33 Å), are shown in

wireframe (teal). Figures generated by PyMOL Molecular Graphics System, Version 1.5.0.4 Schrödinger, LLC.

Table 1. Radiation induced formation of 8-oxo-dG, 8-oxo-dA, and tandem cyclopurine (5'*S*-cdG : 5'*R*-cdG : 5'*S*-cdA : 5'*S*-cdA) lesions in G-quadruplex folded and non-folded states in saturated N_2O (100%). Values represent the mean per 10^6 dG (or 10^6 dA) per Gy of γ-irradiation including maximum standard errors in the range from 0 to 60 Gy of irradiation (cf. Figure S2and S3 in Supporting Information).

Lesion	Entry	Lesions / 10^6 dG / Gy in single-stranded ODNs (perchlorate unbuffered)	Lesions / 10^6 dG/ Gy in G-quadruplex ODNs (perchlorate buffered)	ODN
8-oxo-dG	1	21.2 ± 3.3	78.4 ± 15.0	mutTel24
	2	12.7 ± 2.4	13.2 ± 4.9	Tel22[†]
	3	14.4 ± 1.6	39.9 ± 11.3	TG4T
5'*S*-cdG	4	0.08 ± 0.01	0.08 ± 0.01	mutTel24
	5	0.09 ± 0.02	0.06 ± 0.01	Tel22[†]
	6	0.06 ± 0.01	0.06 ± 0.01	TG4T
5'*R*-cdG	7	0.04 ± 0.01	0.16 ± 0.02	mutTel24
	8	0.04 ± 0.01	0.04 ± 0.01	Tel22[†]
	9	0.06 ± 0.01	0.11 ± 0.01	TG4T
8-oxo-dA[#]	10	0.64 ± 0.11	1.24 ± 0.23	mutTel24
	11	0.20 ± 0.11	0.48 ± 0.04	Tel22[†]
	12			TG4T
5'*S*-cdA[#]	13	0.04 ± 0.01	0.10 ± 0.01	mutTel24
	14	0.04 ± 0.01	0.07 ± 0.01	Tel22[†]
	15			TG4T
5'*R*-cdA[#]	16	0.06 ± 0.01	0.14 ± 0.02	mutTel24
	17	0.04 ± 0.01	0.09 ± 0.01	Tel22[†]
	18			TG4T

[†]Tel22 exists as a mixture of unfolded and folded in G-quadruplex structure in a ratio 1:1; [#]dA nucleosides exist only in the end or in the loop and are not taking part in the G-quartets.